6148 *Inorg. Chem.* **2010**, *49*, 6148–6152
DOI: 10.1021/ic1007654

Inorganic Chemistry
Article

Bimetallic Ni−Pt Nanocatalysts for Selective Decomposition of Hydrazine in Aqueous Solution to Hydrogen at Room Temperature for Chemical Hydrogen Storage

Sanjay K. Singh and Qiang Xu*

National Institute of Advanced Industrial Science and Technology (AIST), Ikeda, Osaka 563-8577, Japan

Received April 21, 2010

The design and development of alloy catalysts has been a focus of intense interest because suitable selection and control over the composition of alloy catalysts can result in greatly improved activity and selectivity, while it is unusual that the combination of two inactive metals gives a highly active catalyst. In this work, we found that Ni−Pt bimetallic nanocatalysts, with a platinum content as low as 7 mol %, prepared by the coreduction of the corresponding metal chlorides, exhibit excellent catalytic activity to the decomposition of hydrous hydrazine, producing hydrogen with a 100% selectivity at room temperature, whereas the corresponding single-component nickel and platinum counterparts are inactive for this reaction. These results provide new possibilities for searching heterometallic catalysts. The present catalyst with low noble-metal content promotes the practical use of the hydrogen-storage system based on the catalytic complete decomposition of hydrazine in aqueous solution at ambient conditions.

Introduction

New materials that can solve challenging key hurdles for safe and efficient hydrogen storage are of paramount importance.[1−6] Anhydrous hydrazine, a liquid at room temperature with a hydrogen content as high as 12.5 wt %,[7] could be a competent candidate for hydrogen storage;[8−14] however, its incompatibility with metals is a major hurdle for applying it safely. Recent studies have shown that hydrous hydrazine could be a potential hydrogen-storage material via the complete decomposition reaction (1) at room temperature.[15,16]

$$H_2NNH_2 \xrightarrow[H_2O,\ rt]{catalyst} N_2(g) + 2H_2(g) \quad (1)$$

Hydrazine monohydrate, $H_2NNH_2 \cdot H_2O$, a liquid at room temperature, has a hydrogen-storage capacity (the hydrogen content available for hydrogen generation) as high as 8.0 wt %, meeting the DOE target for hydrogen-storage materials,[6] and is safe in handling.[7] Notably, the only production of nitrogen in addition to hydrogen by the complete decomposition of hydrazine as well as easy recharge with the current available infrastructure of liquid fuel recharge gives high advantages of this material for hydrogen storage.[15,16] Because nitrogen can be transformed to ammonia by the Haber−Bosch process[17] and subsequently to hydrazine on a large scale,[18,19] the key to exploiting hydrazine as a hydrogen-storage material is the development of suitable catalysts that can avoid the undesired reaction pathway (2), and the catalysts should be economically viable.

$$3H_2NNH_2 \rightarrow 4NH_3 + N_2(g) \quad (2)$$

*To whom correspondence should be addressed. E-mail: q.xu@aist.go.jp.

(1) Graetz, J. *Chem. Soc. Rev.* **2009**, *38*, 73.
(2) Hamilton, C. W.; Baker, R. T.; Staubitz, A.; Manners, I. *Chem. Soc. Rev.* **2009**, *38*, 279.
(3) Xiong, Z.; Yong, C. K.; Wu, G.; Chen, P.; Shaw, W.; Karkamkar, A.; Autrey, T.; Jones, M. O.; Johnson, S. R.; Edwards, P. P.; David, W. I. F. *Nat. Mater.* **2008**, *7*, 138.
(4) Chandra, M.; Xu, Q. *J. Power Sources* **2006**, *156*, 190.
(5) Jiang, H.-L.; Singh, S. K.; Yan, J.-M.; Zhang, X.-B.; Xu, Q. *ChemSusChem* **2010**, *3*, 541.
(6) U.S. DOE. Hydrogen, Fuel Cells & Infrastructure Technologies Program Multi-Year Research, Development, and Demonstration Plan, Hydrogen Storage Technical Plan, 2007, http://www1.eere.energy.gov/hydrogenandfuelcells/mypp/.
(7) Schmidt, E. W. *Hydrazine and its Derivatives: Preparation, Properties, Applications*, 2nd ed.; John Wiley & Sons: New York, 1984.
(8) Santos, J. B. O.; Valença, G. P.; Rodrigues, J. A. J. *J. Catal.* **2002**, *210*, 1.
(9) Prasad, J.; Gland, J. L. *Langmuir* **1991**, *7*, 722.
(10) Armstrong, W. E.; Ryland, L. B.; Voge, H. H. U.S. Patent 4,124,538, 1978.
(11) Zheng, M.; Cheng, R.; Chen, X.; Li, N.; Li, L.; Wang, X.; Zhang, T. *Int. J. Hydrogen Energy* **2005**, *30*, 1081.
(12) Chen, X.; Zhang, T.; Zheng, M.; Wu, Z.; Wu, W.; Li, C. *J. Catal.* **2004**, *224*, 473.
(13) Alberas, D. J.; Kiss, J.; Liu, Z.-M.; White, J. M. *Surf. Sci.* **1992**, *278*, 51.
(14) Al-Haydari, Y. K.; Saleh, J. M.; Matloob, M. H. *J. Phys. Chem.* **1985**, *89*, 3286.
(15) Singh, S. K.; Xu, Q. *J. Am. Chem. Soc.* **2009**, *131*, 18032.
(16) Singh, S. K.; Zhang, X.-B.; Xu, Q. *J. Am. Chem. Soc.* **2009**, *131*, 9894.
(17) Smil, V. *Enriching the Earth: Fritz Haber, Carl Bosch and the Transformation of World Food Production*; MIT Press: Cambridge, MA, 2001.
(18) Hayashi, H. *Catal. Rev.−Sci. Eng.* **1990**, *32*, 229.
(19) Hayashi, H. *Res. Chem. Intermed.* **1998**, *24*, 183.

Published on Web 06/02/2010

Recently, we have found that alloying nickel, which itself is inactive for this reaction, with rhodium in a 1:4 (Ni/Rh) molar ratio drastically enhances the selectivity to 100% for the generation of hydrogen by the complete decomposition of hydrazine in aqueous solution at room temperature.[15] Here, we report that the Ni−Pt bimetallic alloy nanocatalyst, with a platinum content of 7−31 mol %, exhibits excellent catalytic activity to the decomposition of hydrazine in aqueous solution, producing hydrogen with 100% selectivity at room temperature in contrast to the corresponding single-component nickel and platinum counterparts, which are inactive for this reaction. It is noteworthy that the content of the noble metal (platinum) can be lowered to a value as low as 7 mol % in comparison to the value of 80 mol % for rhodium, which is more expensive than platinum, in the Rh_4Ni catalyst.

Experimental Section

General Considerations. Commercial chemicals were used as received for catalyst preparation and hydrazine decomposition experiments. Hydrazine monohydrate ($H_2NNH_2 \cdot H_2O$, 99%), sodium borohydride ($NaBH_4$, 99%), hexadecyltrimethylammonium bromide (CTAB, 95%), and $FeCl_2 \cdot 4H_2O$ (95%) were obtained from Aldrich. K_2PtCl_4, $CoCl_2 \cdot 6H_2O$ (99.5%), $NiCl_2 \cdot 6H_2O$ (99.9%), $CuCl_2$ (95%), and NiO were purchased from Wako. $PtO_2 \cdot xH_2O$ (78.8%) was purchased from Mitsuwa Chemicals. Mass analysis of the generated gases was performed using a Balzers Prisma QMS 200 mass spectrometer. Powder X-ray diffraction (XRD) studies were performed on a Rigaku RINT-2000 X-ray diffractometer (Cu Kα). Scanning electron microscopy (SEM; Hitachi S-5000) and transmission electron microscopy (TEM; FEI TECNAI G^2) with selected area electron diffraction (SAED) and energy-dispersive X-ray detection (EDS) were applied for detailed microstructural information. The SEM and TEM samples were prepared by depositing a few droplets of the nanoparticle suspension onto the amorphous carbon-coated copper grids, which were dried under an argon atmosphere. Surface area measurements were performed by dinitrogen adsorption at liquid-nitrogen temperature using automatic volumetric adsorption equipment (Belsorp II). ^{15}N NMR spectra were recorded on a JEOL JNM-AL400 spectrometer at an operating frequency of 40.40 MHz. Liquid samples were contained in 5.0-mm-o.d. sample tubes, in which coaxial inserts containing CD_3CN (^{15}N, δ −134.00 ppm) as an external reference and a lock were placed. X-ray photoelectron microscopy (XPS) analysis was carried out on a Shimadzu ESCA-3400 X-ray photoelectron spectrometer using a Mg Kα source (10 kV, 10 mA). Argon sputtering experiments were carried out under the conditions of background vacuum = 3.2×10^{-6} Pa and sputtering acceleration voltage = 1 kV. The atomic composition of $Ni_{0.93}Pt_{0.07}$ was analyzed by means of an inductively coupled plasma (ICP) spectrometer (Rigaku, CIROS-120EOP).

Preparation of $Ni_{1-x}Pt_x$ (x = 0.03−0.74) Nanocatalysts. A series of $Ni_{1-x}Pt_x$ nanocatalysts (x = 0.03−0.74) were synthesized using a surfactant-aided coreduction method, where x represents the molar portion of platinum. A typical synthetic procedure for $Ni_{0.93}Pt_{0.07}$ is described here. To a 2.5 mL aqueous suspension of $NiCl_2 \cdot 6H_2O$ (0.058 g, 0.245 mmol), K_2PtCl_4 (0.008 g, 0.019 mmol), and CTAB (0.105 g, 0.288 mmol), obtained by subsequent sonication and stirring for 5 min, was added dropwise a 1.5 mL aqueous solution of $NaBH_4$ (0.020 g, 0.526 mmol). The contents of the flask is vigorously shaken for 2 min, resulting in the generation of a $Ni_{0.93}Pt_{0.07}$ nanocatalyst as a black suspension, which was used for the catalytic reaction. The amounts of $NiCl_2 \cdot 6H_2O$ and K_2PtCl_4 used for the preparation of $Ni_{1-x}Pt_x$ were 0.065 g (0.274 mmol) and 0.004 g (0.010 mmol) for $Ni_{0.97}Pt_{0.03}$, 0.050 g (0.211 mmol) and 0.011 g (0.027 mmol) for $Ni_{0.89}Pt_{0.11}$, 0.043 g (0.181 mmol) and 0.015 g (0.036 mmol) for $Ni_{0.83}Pt_{0.17}$, 0.036 g (0.152 mmol) and 0.019 g (0.046 mmol) for $Ni_{0.77}Pt_{0.23}$, 0.029 g (0.122 mmol) and 0.023 g (0.055 mmol) for $Ni_{0.69}Pt_{0.31}$, 0.022 g (0.093 mmol) and 0.027 g (0.065 mmol) for $Ni_{0.59}Pt_{0.41}$, 0.014 g (0.059 mmol) and 0.030 g (0.072 mmol) for $Ni_{0.45}Pt_{0.55}$, and 0.007 g (0.029 mmol) and 0.034 g (0.082 mmol) for $Ni_{0.26}Pt_{0.74}$.

Preparation of Monometallic Nickel and Platinum Nanocatalysts. A synthetic procedure analogous to that for the $Ni_{0.77}Pt_{0.23}$-nanocatalyst was adapted, using only $NiCl_2 \cdot 6H_2O$ (0.072 g, 0.304 mmol) and K_2PtCl_4 (0.038 g, 0.092 mmol) respectively for the preparation of monometallic nickel and platinum nanocatalysts.

Preparation of Ni@Pt Core−shell Nanocatalysts. A 2.5 mL aqueous solution of $NiCl_2 \cdot 6H_2O$ (0.036 g, 0.152 mmol) and CTAB (0.105 g, 0.288 mmol) was added to a 1.5 mL of aqueous solution of $NaBH_4$ (0.020 g, 0.526 mmol), which was then vigorously stirred and shaked to obtain a black suspension. The nickel nanoparticles were collected by centrifugation (15 000 rpm, 20 min, 298 K) and dried for 8 h at 363 K. The obtained nickel nanoparticles were dispersed in a 4.0 mL aqueous solution of K_2PtCl_4 (0.019 g, 0.046 mmol) by sonication, and the resulting suspension was kept at room temperature for 8 h. The Ni@Pt core−shell nanoparticles thus obtained were collected by centrifugation (15 000 rpm, 20 min, 298 K) and dried for 8 h at 363 K.

Preparation of Nickel and Platinum Physical Mixture Nanocatalysts. Separately synthesized monometallic nickel and platinum nanoparticles were mixed together in an equimolar ratio and dispersed in 4.0 mL of distilled water before being used for the catalytic reaction.

Preparation of $M_{0.77}Pt_{0.23}$ (M = Fe, Co, and Cu) Nanocatalysts. A synthetic procedure similar to that for $Ni_{0.77}Pt_{0.23}$ was adapted to synthesize $M_{0.77}Pt_{0.23}$ (M = Fe, Co, and Cu) nanocatalysts using $FeCl_2 \cdot 4H_2O$ (0.031 g, 0.156 mmol), $CoCl_2 \cdot 6H_2O$ (0.036 g, 0.152 mmol), and $CuCl_2$ (0.020 g, 0.150 mmol), respectively, in place of $NiCl_2 \cdot 6H_2O$.

Catalytic Hydrazine Decomposition Experiments. Catalytic reactions were carried out at room temperature using a two-neck, round-bottomed flask, with one of the flask openings connected to a gas buret and another used for the introduction of hydrazine monohydrate. The catalytic decomposition reaction of hydrazine for the release of hydrogen (along with nitrogen) was initiated by stirring the mixture of hydrazine monohydrate (0.1 mL, 1.97 mmol), which was introduced by using a syringe to the reaction flask containing a 4.0 mL aqueous suspension of 0.017 g of nanocatalysts (prepared as described above). The gases released during the reaction were passed through a trap containing 1.0 M hydrochloric acid to ensure absorption of ammonia, if produced, of which the volume was monitored using the gas buret. For preparation of the samples for mass spectrometry (MS) and ^{15}N NMR measurements, no trap containing hydrochloric acid was used. Catalyst stability experiments were conducted over the same catalyst by adding an additional equivalent amount of $N_2H_4 \cdot H_2O$ to the reaction vessel after completion of the previous catalytic run.

Characterization of Nanocatalysts. After the hydrazine decomposition reaction, the suspension was centrifuged (15 000 rpm, 10 min, 298 K) to separate the solution and nanocatalyst, which was washed twice with 5.0 mL of water and ethanol, dried at 373 K for 8 h, and then used for SEM, TEM, XPS, and powder XRD measurements.

Results and Discussion

A facile surfactant-aided coreduction synthetic approach was adopted for the preparation of the bimetallic $Ni_{1-x}Pt_x$ (x = 0.03−0.74) nanocatalysts with various compositions of nickel and platinum, which were generated as a black suspension by the coreduction of an aqueous solution of $NiCl_2 \cdot 6H_2O$ and K_2PtCl_4 using an aqueous solution of sodium borohydride as the reducing agent in the presence of surfactant

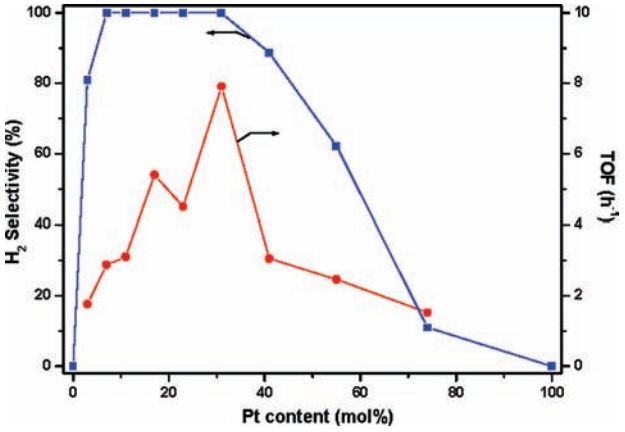

Figure 1. Selectivities and TOFs for hydrogen generation by the decomposition of hydrazine in aqueous solution (0.5 M) catalyzed by nickel, platinum, and $Ni_{1-x}Pt_x$ ($x = 0.03-0.74$) nanocatalysts at room temperature (catalyst = 0.017 g; $N_2H_4 \cdot H_2O$ = 0.1 mL). TOFs were calculated on the basis of the data at 50% completion of the catalytic hydrazine decomposition reaction.

CTAB. Monometallic nickel and platinum nanoparticles were prepared from $NiCl_2 \cdot 6H_2O$ and K_2PtCl_4, respectively, via an analogous procedure. A physical mixture of monometallic nickel and platinum nanoparticles was made by mixing the separately prepared single-component nanoparticles. The catalytic hydrazine decomposition reaction was initiated by introducing hydrazine monohydrate into the reactor containing an aqueous suspension of catalysts. For all of the Ni−Pt nanocatalysts, gas release was initiated immediately with the addition of hydrazine monohydrate, and the amount of resulting gas was measured volumetrically for evaluation of the selectivity toward hydrogen while the gas compositions were identified by MS.

To investigate the dependence of the hydrogen selectivity on the Ni/Pt ratio, $Ni_{1-x}Pt_x$ nanocatalysts with a wide range of platinum contents, 3−74 mol %, were examined (Figure 1). It is found that the Ni−Pt nanocatalysts with platinum contents in the range of 7−31 mol % exhibit 100% hydrogen selectivity. In contrast to the slight decrease in the hydrogen selectivity to 81% with a decrease in the platinum content to 3 mol %, a sharp decrease in the hydrogen selectivity to 28% with an increase in the platinum content to 74 mol % was observed. To our surprise, single-component nickel and platinum nanoparticles, synthesized under analogous reaction conditions, are catalytically inactive to the hydrazine decomposition in aqueous solution.[16] Turnover frequencies (TOFs; h^{-1}) for the catalytic decomposition reaction of hydrazine in aqueous solution over Ni−Pt nanocatalysts (platinum content 3−74 mol %) have been calculated and plotted in Figure 1, which indicated that TOFs of the catalysts vary in the range of 1.5 ($Ni_{0.26}Pt_{0.74}$) to 7.9 h^{-1} ($Ni_{0.69}Pt_{0.31}$).

The $Ni_{1-x}Pt_x$ nanocatalysts with 7−31 mol % platinum contents exhibit analogous time course profiles, releasing 3.0 equiv of gases (Figure S1 in the Supporting Information, SI).[20] For $Ni_{0.93}Pt_{0.07}$, a release of 3.0 equiv of gases was observed in 190 min (Figure 2), which were identified by MS to be hydrogen and nitrogen with a H_2/N_2 ratio of 2.0 (Figure 3). The volumetric and MS results are in agreement with 100% selectivity for hydrogen and nitrogen according to

(20) See the Supporting Information for details.

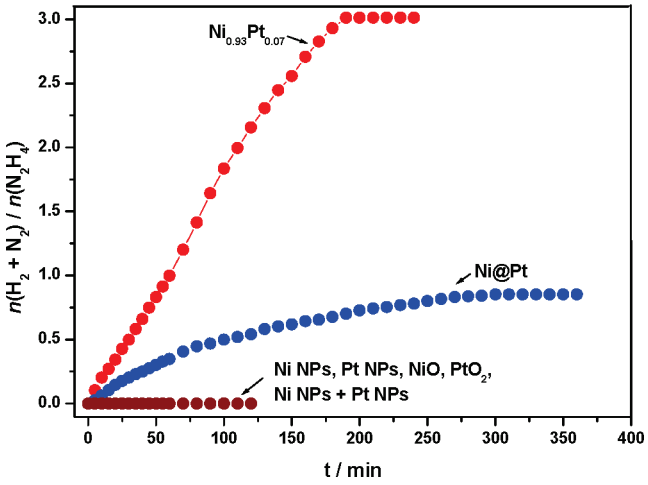

Figure 2. Time course plots for hydrogen generation by the decomposition of hydrazine in aqueous solution (0.5 M) catalyzed by nickel, platinum, $Ni_{0.93}Pt_{0.07}$, Ni@Pt core−shell, NiO, PtO_2, and a physical mixture of monometallic nickel and platinum nanoparticles (catalyst = 0.017 g; $N_2H_4 \cdot H_2O$ = 0.1 mL).

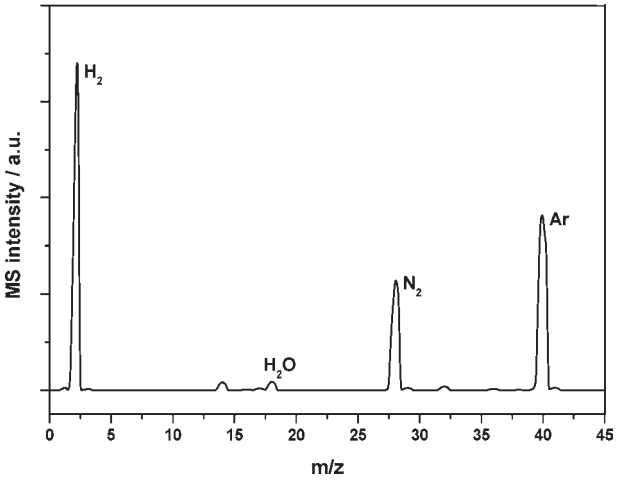

Figure 3. MS profile for the gases from the decomposition reaction of hydrazine in aqueous solution (0.5 M) over the $Ni_{0.93}Pt_{0.07}$ nanocatalyst (catalyst = 0.017 g, $N_2H_4 \cdot H_2O$ = 0.1 mL) detected by a mass spectrometer under an argon atmosphere at room temperature.

eq 1, indicating the complete decomposition of hydrazine in aqueous solution into hydrogen and nitrogen at room temperature. Furthermore, it is found that the hydrogen selectivity is independent of the concentration of hydrazine (Figure S2 in the SI).[20] In addition to the above results, the absence of a ^{15}N NMR signal for ammonia in the solution after the decomposition of hydrazine (Figure S3 in the SI) also supports the complete decomposition of hydrazine to hydrogen and nitrogen.[20] In addition, we have examined the activity and selectivity of $Ni_{0.93}Pt_{0.07}$ for the decomposition of hydrazine in aqueous solution during repeated use, and no significant changes were observed for five runs (Figure S4 in the SI).

In contrast to the high activity observed for the Ni−Pt alloy nanocatalyst, the physical mixture of the monometallic nickel and platinum nanoparticles is catalytically inactive, whereas the Ni@Pt core−shell nanoparticles exhibit poor activity via reaction pathway (1), with which only 0.82 equiv of gases is released, corresponding to ~18% hydrogen selectivity, indicating the involvement of the bimetallic phase

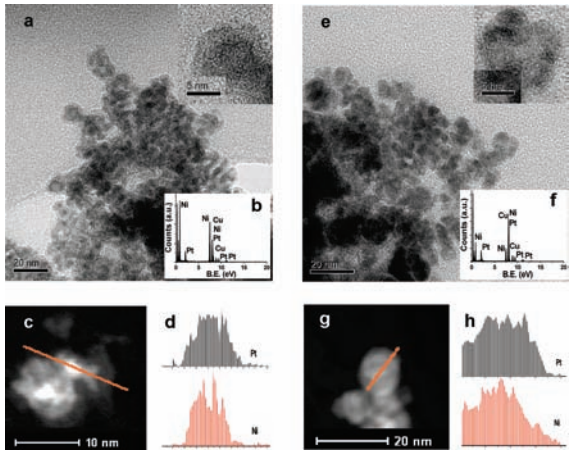

Figure 4. (a and e) TEM images with corresponding HRTEM images (insets), (b and f) EDS spectra (copper signals in EDS are from copper grids), and (c and g) HAADF-STEM images with corresponding (d and h) cross-sectional compositional profiles of $Ni_{0.93}Pt_{0.07}$ and $Ni_{0.77}Pt_{0.23}$ nanocatalysts after being used for the catalytic reaction, respectively.

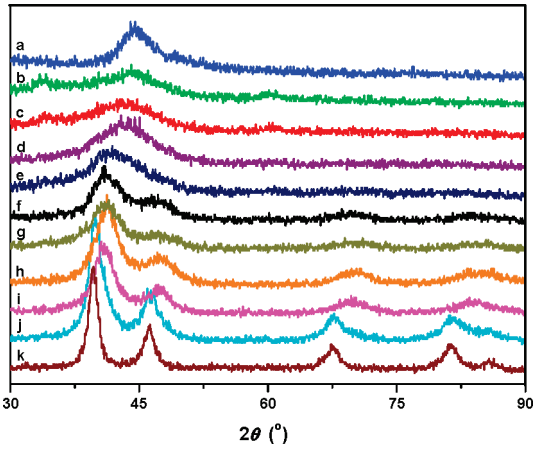

Figure 5. Powder XRD patterns of (a) nickel, (b) $Ni_{0.97}Pt_{0.03}$, (c) $Ni_{0.93}Pt_{0.07}$, (d) $Ni_{0.89}Pt_{0.11}$, (e) $Ni_{0.83}Pt_{0.17}$, (f) $Ni_{0.77}Pt_{0.23}$, (g) $Ni_{0.69}Pt_{0.31}$, (h) $Ni_{0.59}Pt_{0.41}$, (i) $Ni_{0.45}Pt_{0.55}$, (j) $Ni_{0.26}Pt_{0.74}$, and (k) platinum nanocatalysts.

as active species on the catalyst surface and that the synergic interaction between nickel and platinum is necessary for the catalytic activity (Figure 2). Contribution from the nickel or platinum oxide to the observed activity of the Ni−Pt nanocatalyst has been excluded as we have found that NiO, PtO_2, and a mixture of NiO and PtO_2 are inactive for the decomposition of hydrazine in aqueous solution under analogous reaction conditions. Moreover, the analogously synthesized $M_{0.77}Pt_{0.23}$ (M = Fe, Co, and Cu) nanocatalysts exhibit poor or no activity for hydrazine decomposition in aqueous solution, indicating that alloying of the iron, cobalt, and copper metals with platinum has no positive effects on the hydrogen selectivity, in contrast with the drastically positive effect from nickel (Figure S5 in the SI).[20]

The TEM images of the $Ni_{0.93}Pt_{0.07}$ (Figure 4a) and $Ni_{0.77}Pt_{0.23}$ (Figure 4e) catalysts show the nanoparticle agglomerated. The high-resolution TEM (HRTEM; Figure 4b,f) and the corresponding SAED (Figure S6 in the SI) patterns indicate the crystalline nature of these Ni−Pt nanoparticles.[20] TEM and EDS (Figure 4b,g) point analysis of the randomly chosen nanoparticles exhibits the presence of both nickel and platinum with approximate Ni/Pt atomic ratios of 91:9 and 76:24, respectively, for $Ni_{0.93}Pt_{0.07}$ and $Ni_{0.77}Pt_{0.23}$. The Ni/Pt atomic ratio of the $Ni_{0.93}Pt_{0.07}$ catalyst has been confirmed by ICP measurements (91.4:8.6 Ni/Pt). The uniform composition of the bimetallic Ni−Pt nanocatalyst was further confirmed by a line-scan EDS analysis (Figure 4d,h) across the nanoparticles of $Ni_{0.93}Pt_{0.07}$ and $Ni_{0.77}Pt_{0.23}$, which shows no segregation of platinum or nickel in the particles. Furthermore, no significant change in the Ni−Pt nanoparticle morphology or composition was observed during the catalytic reaction (Figures 4 and S7 in the SI). The TEM and HRTEM images (Figure S7 in the SI) of the $Ni_{0.93}Pt_{0.07}$ nanoparticles before the catalytic reaction show an average particle size of ∼5 nm. The EDS point analysis of various nanoparticles chosen randomly exhibits the presence of both nickel and platinum on the same spot with an average atomic composition of 92:8. Crystalline structures of the prepared Ni−Pt nanocatalysts were analyzed using powder XRD (Figure 5).[20] The XRD profiles of the Ni−Pt nanocatalysts with ≥23 mol % platinum show face-centered cubic (fcc) diffraction peaks similar to that of platinum, with a compressed lattice for $Ni_{0.77}Pt_{0.23}$ (a = 3.820 Å). The 2θ values for $Ni_{0.77}Pt_{0.23}$ at 40.88°, 47.20°, 69.64°, and 83.48° can be indexed to diffraction planes of (111), (200), (220), and (311), respectively, corresponding to those of platinum (PDF 65-2868). The Ni−Pt nanocatalysts with lower platinum contents (≤17 mol %) show diffraction peaks similar to those of nickel (PDF 65-0380), with only a visible prominent peak corresponding to that of the (111) plane for nickel (Figure 5). As expected, the diffraction peaks of all of the Ni−Pt nanocatalysts shift to lower angle compared to that of nickel nanoparticles, clearly indicating the alloy formation where the lattice expansion occurred due to substitution of larger platinum atoms for the smaller nickel atoms. The consistency in shift of diffraction peaks to lower angle compared to nickel nanoparticles with an increase in the nickel content excludes any possible segregation of alloy particles, nickel nanoparticles, or platinum particles on the surface.[21−23] The XRD profile (Figure S8 in the SI) of the Ni@Pt nanoparticles also shows fcc diffraction peaks for the platinum shell with a lattice parameter of 3.893 Å.[20]

XPS spectra for the bimetallic $Ni_{1-x}Pt_x$ nanocatalysts exhibit characteristic signals for Ni^0 and Pt^0 (Figure S9 in the SI),[20] indicating the coexistence of both metals in the Ni−Pt nanocatalysts. The observed thin oxide cover on the surface was presumably formed during exposure of the sample to air and was readily removed by argon sputtering of about 6 min (Figures S9 and S10 in the SI). The signals corresponding to metallic nickel and platinum for the Ni $2p_{3/2}$ and Pt $4f_{7/2}$ levels in $Ni_{0.93}Pt_{0.07}$ and $Ni_{0.77}Pt_{0.23}$ nanocatalysts appear at 851.72 (Ni^0) and 71.70 eV (Pt^0) and at 851.32 (Ni^0) and 71.55 eV (Pt^0), respectively. The Pt $4f_{7/2}$ levels for the bimetallic Ni−Pt nanocatalysts are shifted to higher binding energies relative to that for the monometallic platinum sample and the Ni $2p_{3/2}$ levels are shifted to lower energies relative to the monometallic nickel sample (Table S1 in the SI).[24] The electronic compositions and remarkable shifts in

(21) Liu, R.; Ley, K. L.; Pu, C.; Fan, O.; Leyarovska, N.; Segre, C.; Smotkin, E. S. Bifunctional Pt−Ru−Os ternary alloys—improved Pt-based anode for direct methanol fuel cells. In *Electrode Processes VI*; Wieckowski. A., Itaya, K., Eds.; The Electrochemical Society: Pennington, NJ, 1996; pp 341.
(22) Deivaraj, T. C.; Chen., W.; Lee, J. Y. *J. Mater. Chem.* **2003**, *13*, 2555.
(23) Mathiyarasu, J.; Remona, A. M.; Mani, A.; Phani, K. L. N.; Yegnaraman, V. *J. Solid State Electrochem.* **2004**, *8*, 968.

the relative binding energies for the Ni−Pt nanocatalysts are consistent with the alloy formation. Furthermore, the uniformity of the Ni−Pt alloy nanoparticles is confirmed by a nearly constant Ni/Pt ratio from the surface to the core in the XPS spectra with argon sputtering, in accordance with EDS and TEM observations. No chlorine and boron species were detected in the XPS measurements. In addition, the nitrogen adsorption−desorption isotherms (Figure S11 in the SI) of the Ni−Pt nanocatalysts reveal that the Brunauer−Emmett−Teller (BET) surface areas are 28.7, 51.0, 33.5, 28.2, and 56.0 $m^2\ g^{-1}$, respectively, for the $Ni_{0.69}Pt_{0.31}$, $Ni_{0.77}Pt_{0.23}$, $Ni_{0.83}Pt_{0.17}$, $Ni_{0.89}Pt_{0.11}$, and $Ni_{0.93}Pt_{0.07}$ nanocatalysts.

Because the electronic and structural properties of the catalyst surfaces are closely related to their catalytic activities, the precise modification of the catalyst surfaces by the introduction of a second component or change of the morphology could facilitate tuning of the catalytic performance.[25−30] Generally, alloy materials have distinct interactions with the reactant molecules in comparison with the corresponding monometallic catalysts. The formation of heterometallic bonds with strong metal−metal interactions might tune the bonding pattern of the catalyst surface to the reactant molecules and stabilize the possible reaction intermediates, leading to improved catalytic activity and selectivity in comparison with those of the corresponding monometallic catalysts.[29−34] The observed high activity and 100% hydrogen selectivity over the Ni−Pt nanocatalysts prepared from the respective inactive monometallic counterparts exhibit a striking feature that the strong interaction between different metals may lead not only to quantitative improvement but also to a qualitative leap of the catalytic performance. It has been reported that, for a palladium-rich Pd_xPt_{1-x} alloy, the electronic structure and interaction between the catalyst surface and substrates can be finely tuned by alloying with various amounts of platinum.[35,36] It was reported that the third-body effect and the d-band center shift effect account for the observed results.[35,36] The present observation of the Ni−Pt alloy nanocatalysts for hydrazine decomposition in aqueous solution exhibits that the bimetallic Ni−Pt nanocatalyst surface has characteristic properties that are distinctly different from those of either platinum or nickel monometallic nanoparticles. Furthermore, considering the uniform composition of the Ni−Pt catalyst, it is reasonable to understand that the alloying of nickel and platinum leads to a modification of the catalyst surface by incorporating considerable intermetallic electronic interaction[35−38] and thereby controls the interaction of the catalyst surface with the hydrazine molecule as well as tunes the stability of the reaction intermediates on the modified catalyst surface.[8,9] Because neither the nickel nor the platinum nanoparticles show catalytic activity in the hydrogen generation from hydrazine, the presence of both metals on the catalyst surface is vital for the catalytic activity. This implies that catalysis requires the existence of two different metal sites on the surface. The coexistence of nickel and platinum on the catalyst surface results in the activation of bonds in hydrazine toward the reaction pathway (1) over pathway (2) for the complete decomposition of hydrazine in aqueous solution to hydrogen and nitrogen.

Conclusions

In summary, we demonstrated that the alloying of nickel and platinum makes it possible to achieve 100% selectivity for the decomposition of hydrazine in aqueous solution to hydrogen at room temperature, whereas the monometallic nickel and platinum counterparts are inactive to this reaction. The bimetallic Ni−Pt nanocatalysts with the platinum content as low as 7 mol % ($Ni_{0.93}Pt_{0.07}$) present a step toward a high-performance catalyst system, which will open a door to exploiting hydrous hydrazine as a highly promising practical material for hydrogen storage.

Acknowledgment. We acknowledge the reviewers for their valuable suggestions and JSPS for financial support. S.K.S. thanks JSPS for a postdoctoral fellowship.

Supporting Information Available: Results for SEM, TEM, XPS, BET, and powder XRD of the nanocatalysts and catalytic hydrazine decomposition experiments in aqueous solution. This material is available free of charge via the Internet at http://pubs.acs.org.

(24) Moulder, J. F.; Chastain, J.; King, R. C. *Handbook of X-ray Photoelectron Spectroscopy: A Reference Book of Standard Spectra for Identification and Interpretation of XPS Data*; Physical Electronics: Eden Prairie, MN, 1995.
(25) Ferrando, R.; Jellinek, J.; Johnston, R. L. *Chem. Rev.* **2008**, *108*, 845.
(26) Stamenkovic, V. R.; Mun, B. S.; Arenz, J. J.; Mayrhofer, M.; Lucas, C. A.; Wang, G.; Ross, P. N.; Markovic, N. M. *Nat. Mater.* **2007**, *6*, 241.
(27) Greeley, J.; Stephens, I. E. L.; Bondarenko, A. S.; Johansson, T. P.; Hansen, H. A.; Jaramillo, T. F.; Rossmeisl, J.; Chorkendorff, I.; Nørskov, J. K. *Nat. Chem.* **2009**, *1*, 552.
(28) Lim, B.; Jiang, M.; Camargo, P. H. C.; Cho, E. C.; Tao, J.; Lu, X.; Zhu, Y.; Xia, Y. *Science* **2009**, *324*, 1302.
(29) Greeley, J.; Mavrikakis, M. *Nat. Mater.* **2004**, *3*, 810.
(30) Rodriguez, J. A.; Goodman, D. W. *Science* **1992**, *257*, 897.
(31) Zhang, X.-B.; Yan, J.-M.; Han, S.; Shioyama, H.; Xu, Q. *J. Am. Chem. Soc.* **2009**, *131*, 2778.
(32) Xie, X.; Li, Y.; Liu, Z.-Q.; Haruta, M.; Shen, W. *Nature* **2009**, *458*, 746.
(33) Yan, J.-M.; Zhang, X.-B.; Han, S.; Shioyama, H.; Xu, Q. *Angew. Chem., Int. Ed.* **2008**, *47*, 2287.
(34) Heemeier, M.; Carlsson, A. F.; Naschitzki, M.; Schmal, M.; Bäumer, M.; Freund, H.-J. *Angew. Chem., Int. Ed.* **2002**, *41*, 4073.
(35) Zhang, H.-X.; Wang, C.; Wang, J.-Y.; Zhai, J.-J.; Cai, W.-B. *J. Phys. Chem. C* **2010**, *114*, 6446.
(36) Wang, C.; Peng, B.; Xie, H.-N.; Zhang, H.-X.; Shi, F.-F.; Cai, W.-B. *J. Phys. Chem. C* **2009**, *113*, 13841.
(37) Stamenkovic, V. R.; Fowler, B.; Mun, B. S.; Wang, G.; Ross, P. N.; Lucas, C. A.; Markovic, N. M. *Science* **2007**, *315*, 493.
(38) Hwu, H. H.; Eng, J., Jr.; Chen, J. G. *J. Am. Chem. Soc.* **2002**, *124*, 702.